Supporting Information Appendix

# Iterative optimization yields Mcl-1–targeting stapled peptides with selective cytotoxicity to Mcl-1–dependent cancer cells

Raheleh Rezaei Araghi[a], Gregory H. Bird[b,c], Jeremy A. Ryan[d], Justin M. Jenson[a], Marina Godes[b,c], Jonathan R. Pritz[b,c], Robert A. Grant[a], Anthony Letai[d], Loren D. Walensky[b,c], and Amy E. Keating[a,e]

[a]Department of Biology, Massachusetts Institute of Technology, Cambridge, MA 02139; [b]Department of Pediatric Oncology, Dana-Farber Cancer Institute, Boston, MA 02215; [c]Linde Program in Cancer Chemical Biology, Dana-Farber Cancer Institute, Boston, MA 02215; [d]Department of Medical Oncology, Dana-Farber Cancer Institute, Boston, MA 02215; and [e]Department of Biological Engineering, Massachusetts Institute of Technology, Cambridge, MA 02139

Contents:

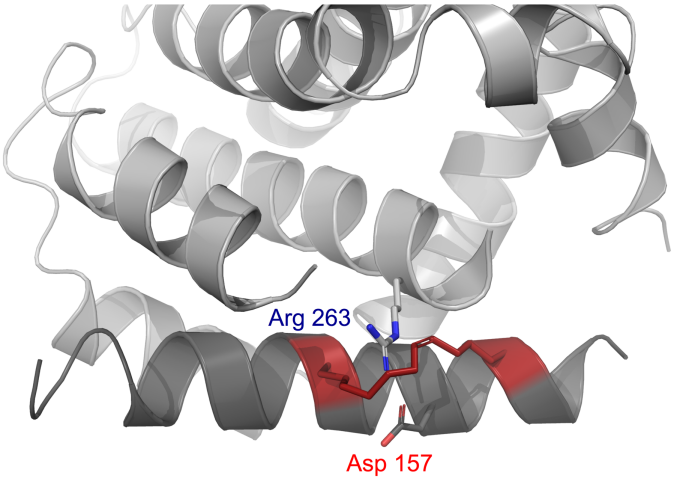


**Figure S1. Model of a low affinity SAH-MB2/Mcl-1 complex.** Based on a docking model built with Bioluminate using 2PQK (1), the *i, i+7* hydrocarbon staple in SAH-MB2-19 (red) is predicted to disrupt a critical salt bridge between Asp 157 of SAH-MB2-19 (Bim numbering) and Arg 263 of Mcl-1.

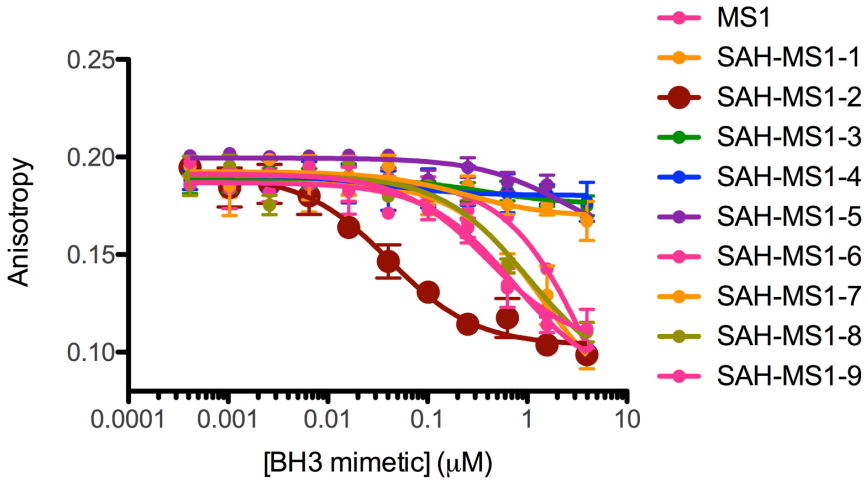


**Figure S2. Fluorescence anisotropy competition binding data for MS1 and SAH-MS1 peptides**. Competition of SAH-MS1 peptides with fluorescently labeled 21-mer Bim BH3 peptide (25 nM) for binding to recombinant Mcl-1 (50 nM). Data are mean ± s.d. for three experiments performed in duplicate. Fitted IC50 values are listed in Table 1.

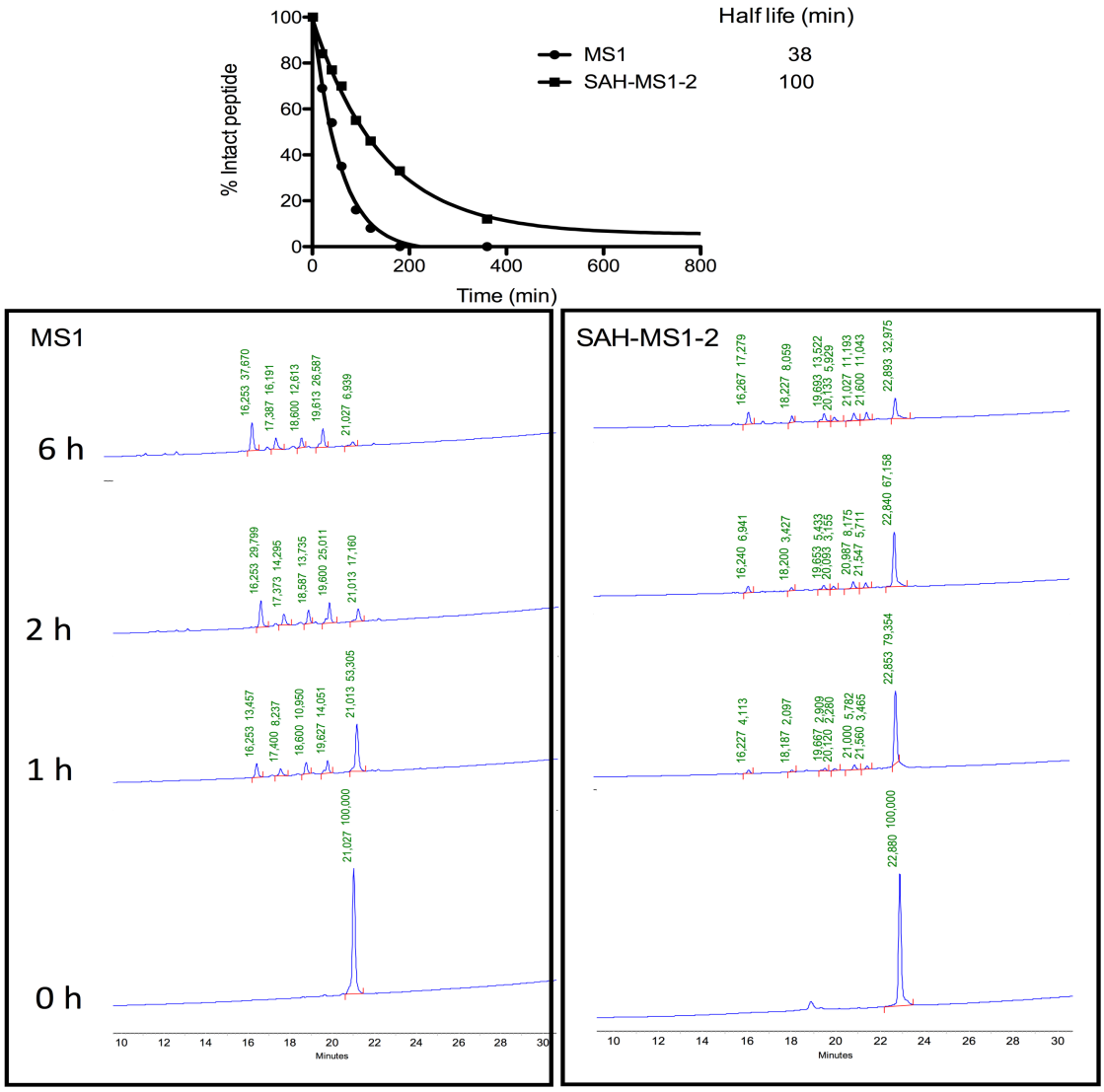


**Figure S3. Proteolytic stability of SAH-MS1-2 compared to MS1.** HPLC profiles and fitted half-lives of MS1 (retention time, r.t. = 21 min) and SAH-MS1-2 (r.t. = 22.8 min) upon exposure to chymotrypsin.

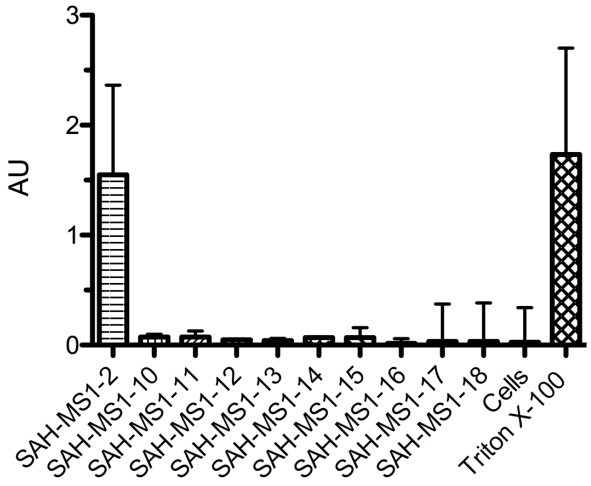


**Figure S4. Optimized SAH-MS1 peptides do not disrupt MEF membranes**. Lactate dehydrogenase (LDH) release assays were performed on SAH-MS-1-treated MEFs in the presence of 10% FBS ([BH3 peptide] = 30 μM). Error bars are mean +/- s.d. for experiments performed two times with independent preparations of cells and BH3 mimetic treatments; duplicate measurements were averaged for each biological replicate.

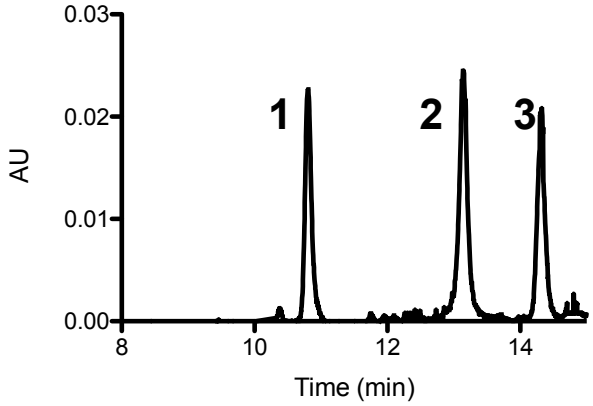


**Figure S5. Peptide modification by stapling increases hydrophobicity.** HPLC profiles of unmodified MS1 (1), SAH-MS1-18 (2), and SAH-MS1-2 (3), as monitored by absorbance at 220 nm.

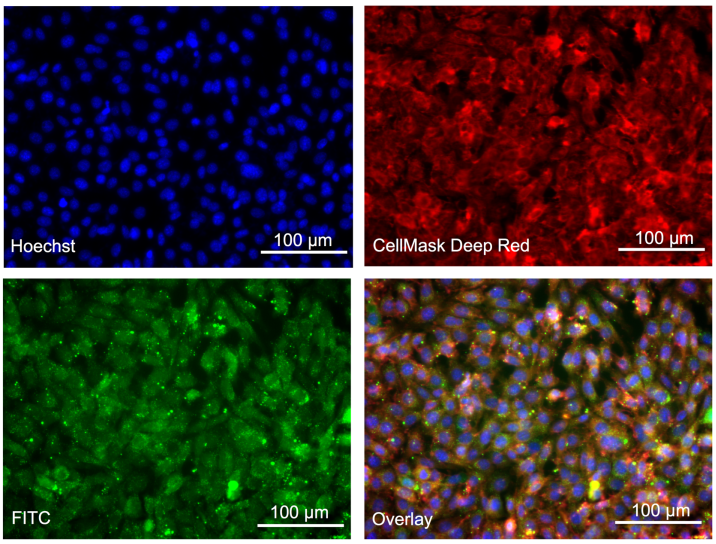


**Figure S6. Cellular uptake of FITC-SAH-MS1-18.** MEFs were treated with FITC-labeled SAH-MS1-18 peptide (green) in the absence of serum, and counterstained with Hoechst 33342 (blue) and Cellmask Deep Red (red).

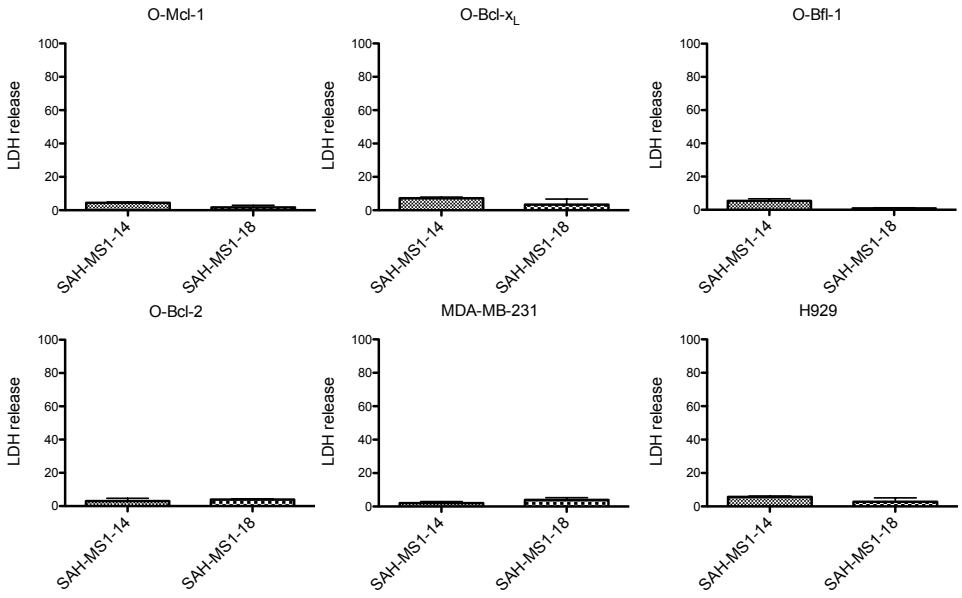


**Figure S7. Optimized SAH-MS1 peptides do not disrupt cancer cell membranes.** LDH release assays were performed on the indicated cell lines treated with 20 μM stapled peptides in the presence of 10% serum. Data were normalized based on the response to treatment with 1% Triton X-100 (100% release) or media alone (0% release). Error bars are mean +/- s.d. for experiments performed two times with independent preparations of cells and BH3 mimetic treatments; duplicate measurements were averaged for each biological replicate.

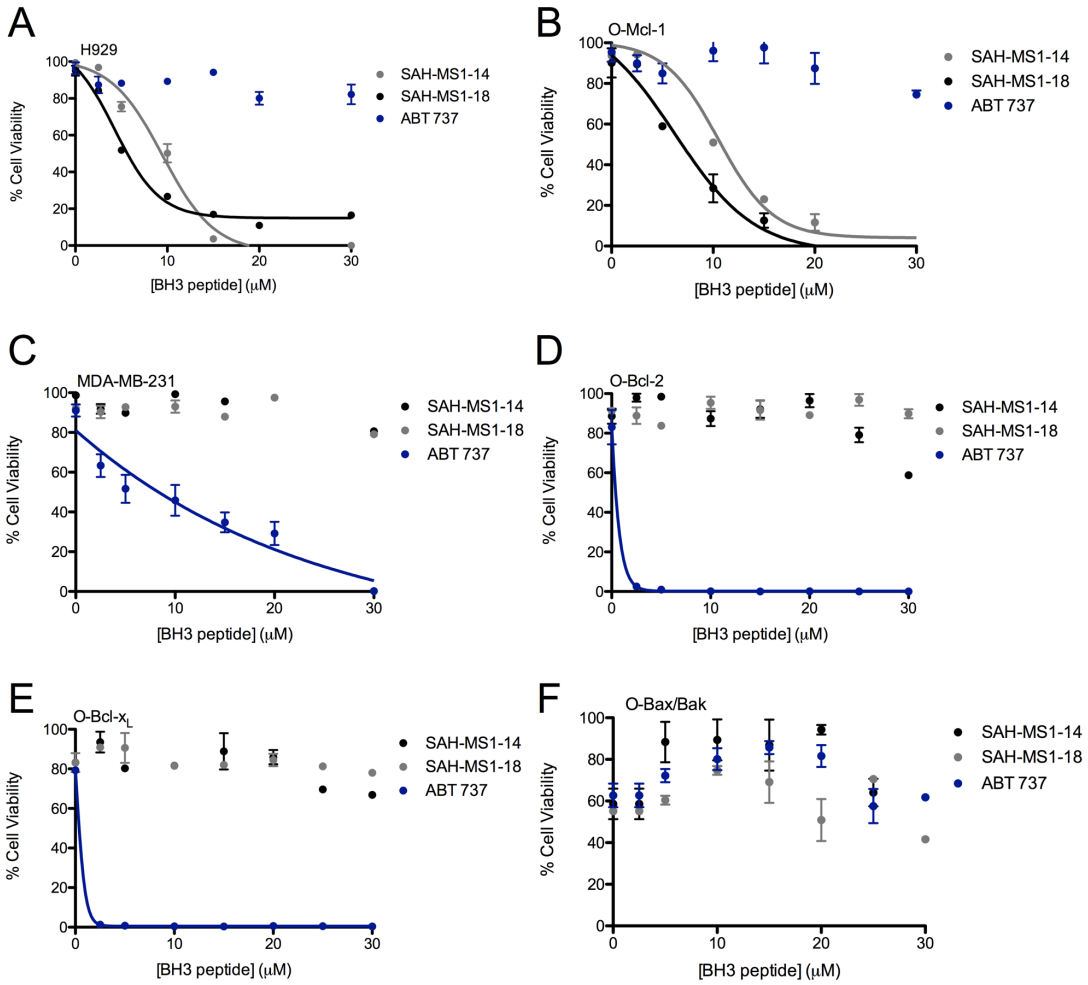


**Figure S8. Selective cytotoxicity of SAH-MS1-14 and SAH-MS1-18 in Mcl-1-dependent cancer cells.** The indicated cancer cells (A: H929, B: O-Mcl-1, C: MDA-MB-231, D: O-Bcl-2, E: O-Bcl-$x_L$ and F: O-Bax/Bak) were exposed to a serial dilution of stapled peptides in media containing 10% serum. Cell viability measured by CTG assay at 24 h revealed dose-responsive and anti-apoptotic blockade-selective cytotoxicity. Error bars are mean +/- s.d. for experiments performed three times with independent preparations of cells and BH3 mimetic treatments; duplicate measurements were averaged for each biological replicate.

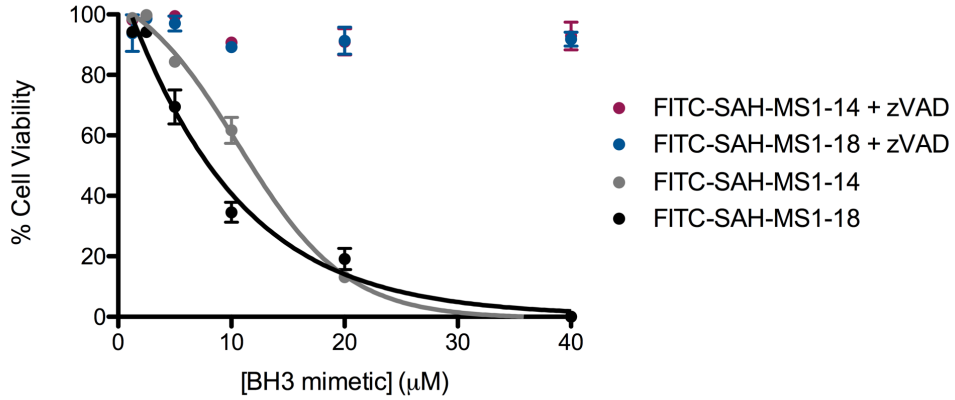


**Figure S9. Selective cytotoxicity of FITC-SAH-MS1-14 and FITC-SAH-MS1-18 in Mcl-1 dependent cancer cells.** O-Mcl-1 cell viability was measured after 24 h incubation with FITC labeled MS1-SAH-14 or MS1-SAH-18 in the presence or absence of the caspase inhibitor zVAD. Error bars are mean +/- s.d. for experiments performed two times with independent preparations of cells and BH3 mimetic treatments; duplicate measurements were averaged for each biological replicate. Fitted EC50 values are 12 ± 0.6 μM and 8 ± 0.8 μM for SAH-MS1-14 and SAH-MS1-18, respectively.

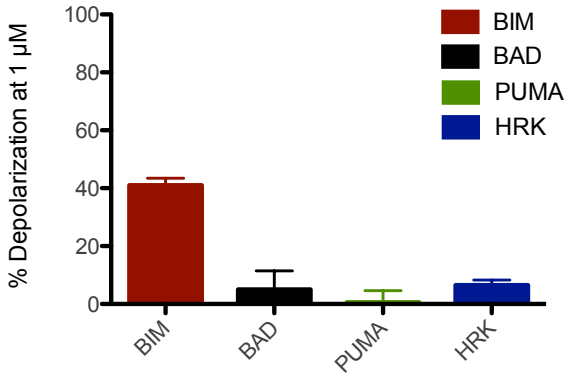


**Figure S10. BH3 profiling of the SF295 cell line using native BH3 peptides** (2)**.** Mitochondria in permeabilized SF295 cells did not depolarize in response to treatment with Hrk, Bad or Puma peptides, but did respond to Bim BH3, which can directly activate Bax or Bak to induce mitochondrial outer membrane permeabilization. Error bars represent mean +/- s.d. for experiments performed in at least duplicate.

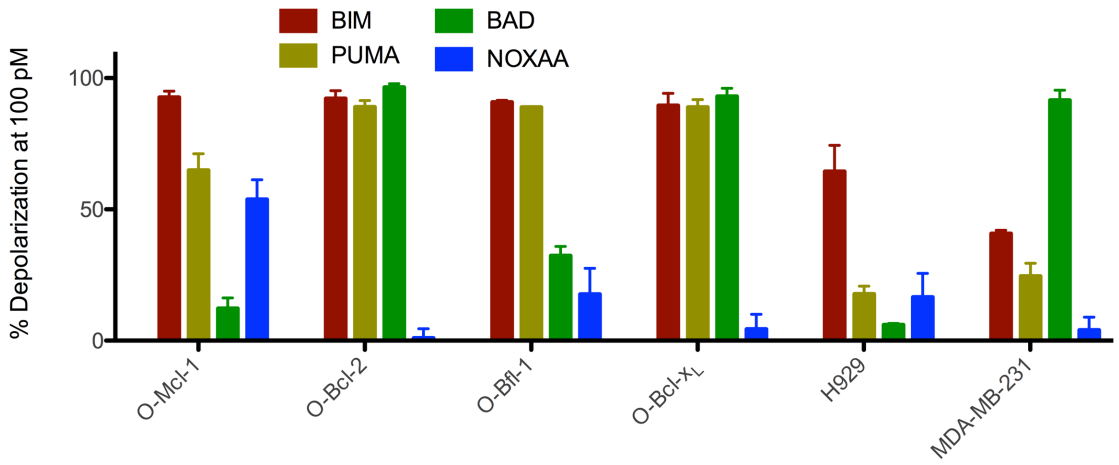


**Figure S11. BH3 profiling of cell lines using native BH3 peptides** (2)**.** Error bars represent mean +/- s.d. for experiments preformed in at least triplicate. Among the natural BH3 peptides, Bim and Puma peptides engage the broadest range of anti-apoptotic targets, whereas NOXA-A and BAD are Mcl-1- and Bcl-2/Bcl-$x_L$-selective, respectively.

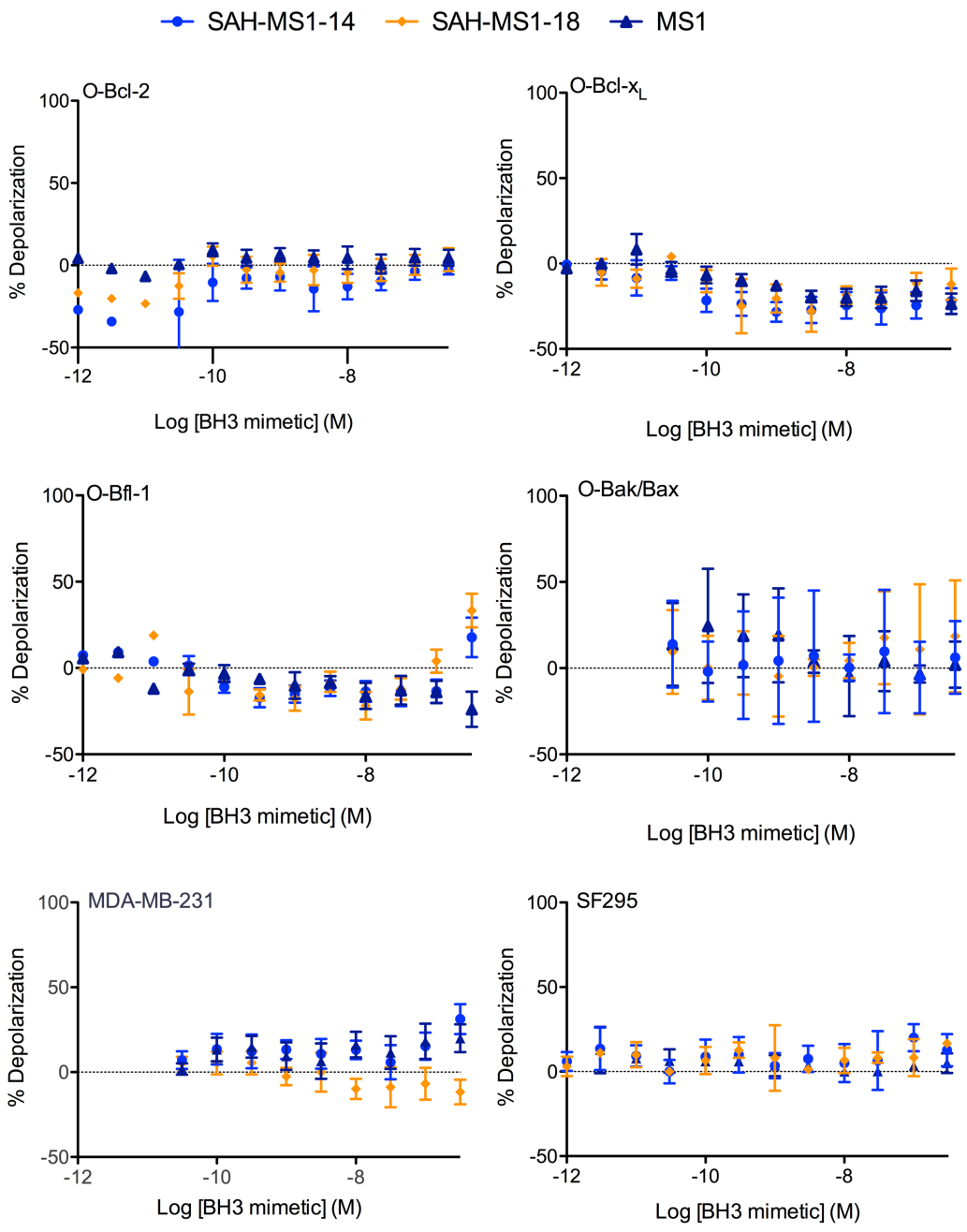


**Figure S12. BH3 profiling of MS1 peptides in cancer cells with a non-Mcl-1 dependent apoptotic blockade.** BH3 profiling was performed on the indicated permeabilized cell lines treated with SAH-MS1 or MS1 peptides. Percent mitochondrial membrane depolarization is reported for each construct. Data are mean +/- s.d. for experiments performed in triplicate.

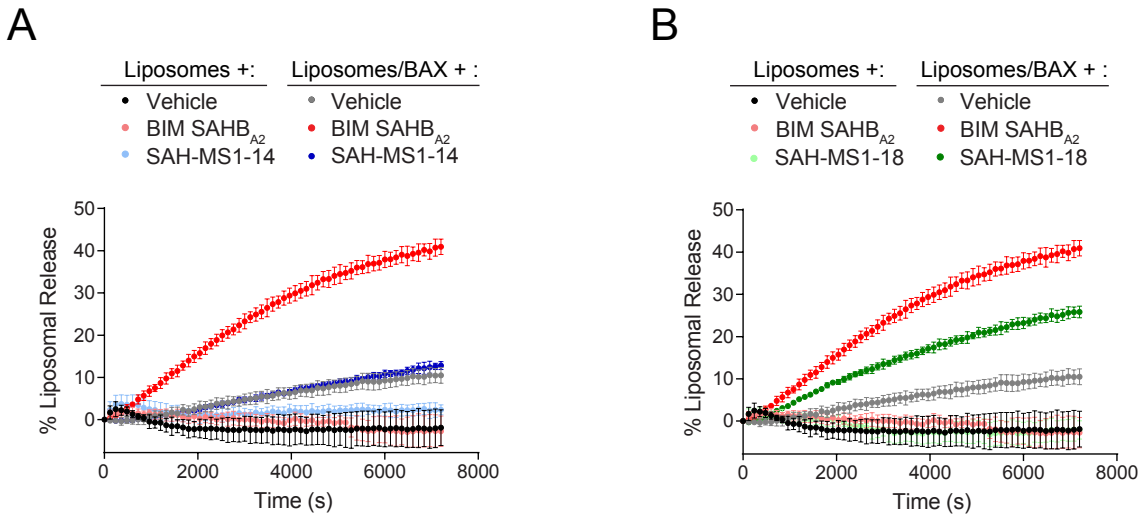


**Figure S13. Assessment of direct Bax activation by SAH-MS1-14 and SAH-MS1-18 peptides.** Whereas Bim SAHB$_{A2}$ (red) directly triggered Bax-mediated liposomal release, (A) SAH-MS1-14 (navy) failed to induce Bax activation and (B) SAH-MS1-18 (green) exhibited reduced activity compared to Bim SAHB$_{A2}$. Vehicle was assay buffer containing 0.5% DMSO. Data are mean ± s.d. for experiments performed in quadruplicate, and repeated three times with independent Bax preparations, yielding similar results. Bax, 500 nM; Bim SAHB$_{A2}$, SAH-MS1-14, and SAH-MS1-18, 250 nM.

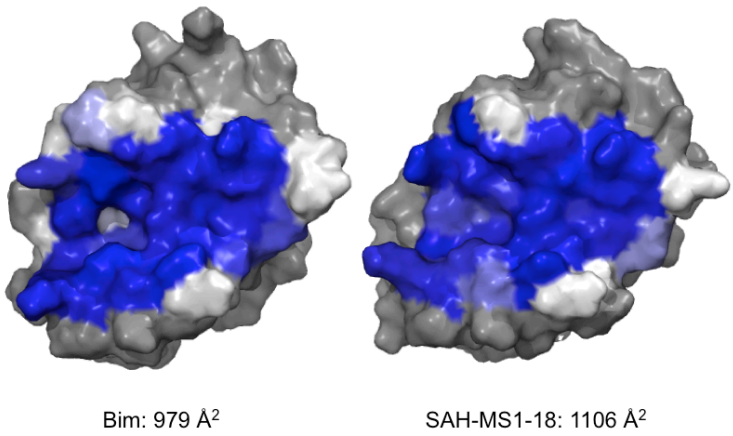


**Figure S14**. **A stapled MS1 peptide buries additional surface area on Mcl-1 compared to unmodified Bim BH3.** Surface area on Mcl-1 that is buried when Mcl-1 is bound to an unmodified Bim BH3 peptide or SAH-MS1-18 is shown in shades of blue. Left, Bim BH3 with sequence GRPEIWIAQELRRIGDEFNAYYA, PDB ID code 2PQK (1). Right, SAH-MS1-18 with sequence IWBXQELXRLGDEINARYAR, PDB ID code 5W89. The peptide is not shown, but would be positioned left-to-right across the blue region on Mcl-1, from N- to C-terminus, in these views.

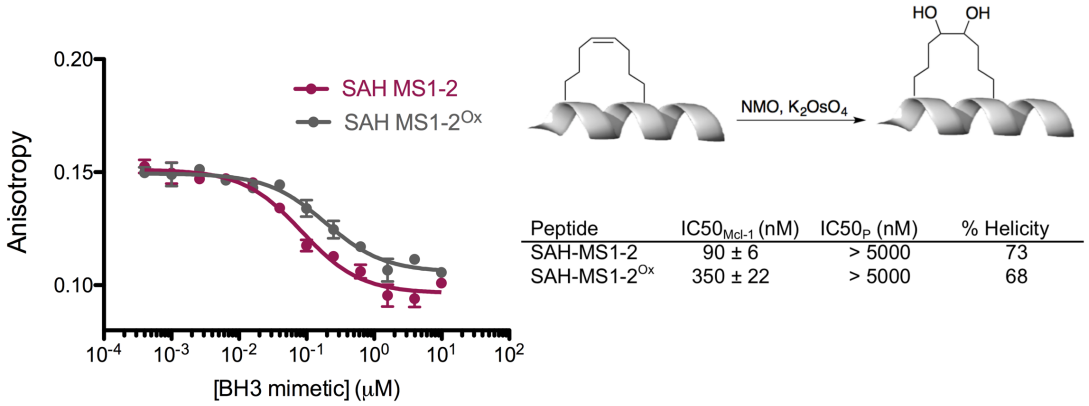


| Peptide | $IC50_{Mcl-1}$ (nM) | $IC50_P$ (nM) | % Helicity |
|---|---|---|---|
| SAH-MS1-2 | 90 ± 6 | > 5000 | 73 |
| SAH-MS1-$2^{Ox}$ | 350 ± 22 | > 5000 | 68 |

**Figure S15. Synthesis and comparative binding activity of SAH-MS1-$2^{Ox}$, a SAH-MS1-2 derivative bearing a dihydroxylated staple.** SAH-MS1-2 and SAH-MS1-$2^{Ox}$ peptides compete with a fluorescently labeled 21-mer Bim-BH3 peptide (25 nM) for binding to Mcl-1 (50 nM) (left). Comparative binding affinities for anti-apoptotic targets, and percent α-helical content as measured by CD, are presented in the table (right). $IC50_P$ indicates the binding affinity for each of the non-Mcl-1 Bcl-2 family anti-apoptotic targets (Bcl-2, Bcl-$x_L$, Bcl-w, Bfl-1). Peptide concentrations were determined using absorbance at 280 nm. Data are mean ± s.d for three experiments performed in duplicate.

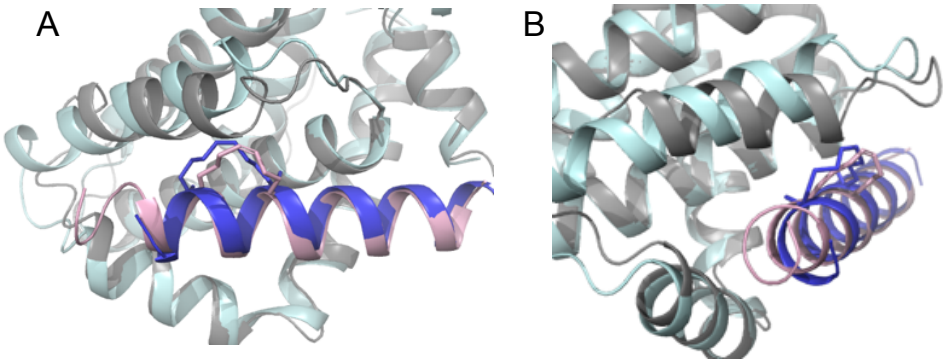


**Figure S16. Predicted vs. observed structures of Mcl-1 bound to SAH-MS1-18.** (A, B) Superposition of a model of the Mcl-1:SAH-MS1-18 complex (Mcl-1 in grey and SAH-MS1-18 in light pink) and the crystal structure (PDB ID code 5W89) (Mcl-1 in light blue and SAH-MS1-18 in dark blue). The staple can be readily accommodated in a docking model built with Bioluminate based on PDB ID code 2PQK (Mcl-1 bound to Bim BH3), requiring little to no conformational change. In contrast, the x-ray structure (PDB ID code 5W89) revealed that SAH-MS1-18 induces significant movement of Mcl-1 α-helix 4.

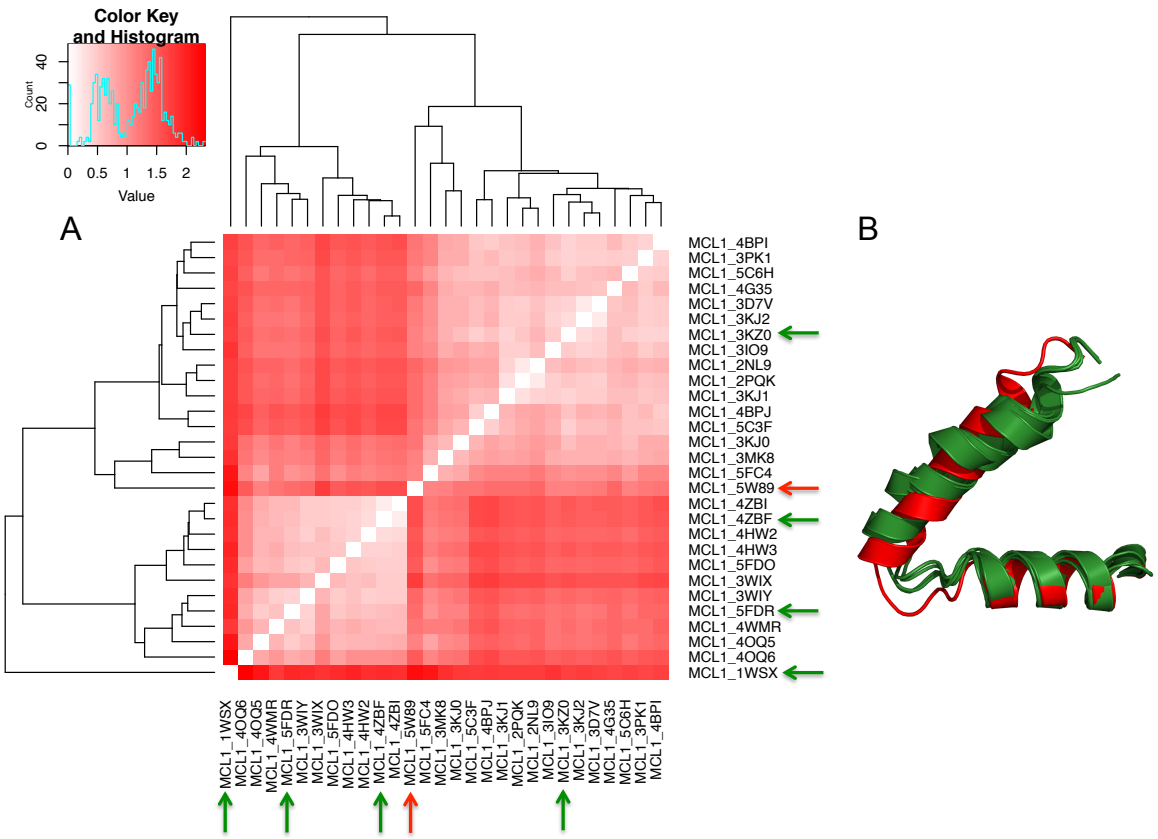


**Figure S17. The distinct conformation of Mcl-1 when bound to SAH-MS1-18, compared to other structures of Mcl-1 bound to BH3 peptides.** (A) Clustergram showing similarities between the conformations of Mcl-1 observed in high-resolution structures of Mcl-1/BH3 peptide complexes. Similarity was measured by pairwise Cα-atom RMSD and is reported in Ångstroms according to the key at the top left, which also shows the distribution of pairwise similarity values. Mcl-1:SAH-MS1-18 (PDB ID code 5W89) is indicated with a red arrow. (B) Superposition of Mcl-1 in the SAH-MS1-18-bound conformation observed in PDB ID code 5W89 (red) compared to four other Mcl-1 conformations in complexes chosen to represent different clusters in the heat map in panel A (green; PDB ID codes 3KZ0 (3), 1WSX (1), 4ZBF (4), and 5FDR (5). The structures included in panel B are indicated with green arrows in panel A.

**Table S1. Biophysical properties of a staple-scanning library of MB2.**

| Peptide | Sequence[a] | $K_{d\ Mcl\text{-}1}$ (nM)[b] | $K_{d\ p}$ (nM)[b] | $IC50_{\ Mcl\text{-}1}$ (nM)[c] | Helicity (%)[d] |
|---|---|---|---|---|---|
| MB2 | IWFAQEIDRIGDEVNAYYARR | 4.7 ± 1.1 | >1000 | > 500 | 22 |
| SAH-MB2-1 | IXFAQXIDRIGDEVNAYYARR | 10.4 ± 3.1 | >1000 | | 30 |
| SAH-MB2-2 | IWXAQEXDRIGDEVNAYYARR | 17.5 ± 2.2 | >1000 | | 87 |
| SAH-MB2-3 | IWFXQEIXRIGDEVNAYYARR | 2.1 ± 1.1 | >1000 | 175 ± 34 | 85 |
| SAH-MB2-4 | IWFAXEIDXIGDEVNAYYARR | 4.2 ± 0.8 | >1000 | | 55 |
| SAH-MB2-5 | IWFAQXIDRXGDEVNAYYARR | 70.9 ± 18.4 | >1000 | | 82 |
| SAH-MB2-6 | IWFAQEXDRIXDEVNAYYARR | >1000 | >1000 | | 48 |
| SAH-MB2-7 | IWFAQEIXRIGXEVNAYYARR | >1000 | >1000 | | 57 |
| SAH-MB2-8 | IWFAQEIDXIGDXVNAYYARR | 9.6 ± 2.7 | >1000 | | 67 |
| SAH-MB2-9 | IWFAQEIDRIXDEVXAYYARR | >1000 | >1000 | | 88 |
| SAH-MB2-10 | IWFAQEIDRIGXEVNXYYARR | 17.7 ± 4.4 | >1000 | | 44 |
| SAH-MB2-11 | IWFAQEIDRIGDXVNAXYARR | 13.6 ± 3.5 | >1000 | | 83 |
| SAH-MB2-12 | IWFAQEIDRIGDEVXAYYXRR | 3.7 ± 1.5 | >1000 | 220 ± 25 | 38 |
| SAH-MB2-13 | I8FAQEIDXIGDEVNAYYARR | 78.8 ± 11.1 | >1000 | | 57 |
| SAH-MB2-14 | IW8AQEIDRXGDEVNAYYARR | >1000 | >1000 | | 54 |
| SAH-MB2-15 | IWF8QEIDRIXDEVNAYYARR | >1000 | >1000 | | 60 |
| SAH-MB2-16 | IWFA8EIDRIGXEVNAYYARR | >1000 | >1000 | | 62 |
| SAH-MB2-17 | IWFAQ8IDRIGDXVNAYYARR | >1000 | >1000 | | 66 |
| SAH-MB2-18 | IWFAQE8DRIGDEXNAYYARR | >1000 | >1000 | | 58 |
| SAH-MB2-19 | IWFAQEI8RIGDEVXAYYARR | >1000 | >1000 | | 60 |
| SAH-MB2-20 | IWFAQEID8IGDEVNXYYARR | >1000 | >1000 | | 55 |
| SAH-MB2-21 | IWFAQEIDR8GDEVNAXYARR | >1000 | >1000 | | 59 |
| SAH-MB2-22 | IWFAQEIDRI8DEVNAYXARR | >1000 | >1000 | | 67 |
| SAH-MB2-23 | IWFAQEIDRIGD8VNAYYAXR | >1000 | >1000 | | 46 |

[a] 8 = (R)-α-7-octenyl alanine, X = (S)-4-pentenylalanine.

[b] Dissociation constants ($K_d$ values) were determined using fluorescence polarization direct binding assays for Mcl-1, Bcl-$x_L$, Bcl-2, Bcl-w, and Bfl-1, as described in the methods.

[c] IC50 values for peptides binding to Mcl-1 were determined as described in Tables 1 and 2.

[d] α-helical content was estimated by circular dichroism at 25 μM peptide concentration in 50 mM Tris buffer pH 7.4.

**Table S2. Biophysical parameters of optimized SAH-MS1 peptides.**

| Peptide | Net charge[a] | % Helicity[b] | Retention time / min[c] |
|---|---|---|---|
| MS1 | +1 | 11 | 10.8 |
| SAH-MS1-2 | +1 | 73 | 14.3 |
| SAH-MS1-10 | 0 | 70 | 14.1 |
| SAH-MS1-11 | -1 | 72 | 13.4 |
| SAH-MS1-12 | -2 | 67 | 13.2 |
| SAH-MS1-13 | 0 | 78 | 13.6 |
| SAH-MS1-14 | +1 | 83 | 13.8 |
| SAH-MS1-15 | 0 | 72 | 13.5 |
| SAH-MS1-16 | -1 | 70 | 13.6 |
| SAH-MS1-17 | +1 | 83 | 13.5 |
| SAH-MS1-18 | 0 | 67 | 13.1 |

Peptide sequences are listed in Table 2.
[a] Net charge indicates formal charge based on standard titration states of residues at pH 7.
[b] $\alpha$-Helicity was estimated from circular dichroism measured using 25 μM peptide in 50 mM Tris buffer pH 7.4.
[c] HPLC retention time was measured at pH 7.0.

**Table S3. Cancer cell lines used in this work and their Bcl-2 paralog dependencies** (6–9).

| Cell line* | Type | Profile | Reference |
|---|---|---|---|
| H929 | Human multiple myeloma cell line | Mcl-1 dependent | Doi: 10.1038/cddis.2014.561 |
| MDA-MB-231 | Human breast cancer cell line | Bcl-$x_L$ dependent | Doi: 10.1073/pnas.0914878107 |
| O-Mcl-1 | (Human Mcl-1) Murine leukemia cell line | Mcl-1 dependent | Doi:10.18632/oncotarget.7204 |
| O-Bcl-$x_L$ | (Human Bcl-$x_L$) Murine leukemia cell line | Bcl-$x_L$ dependent | |
| O-Bcl-2 | (Human Bcl-2) Murine leukemia cell line | Bcl-2 dependent | |
| O-Bfl-1 | (Human Bfl-1) Murine leukemia cell line | Bfl-1 dependent | |
| O-Bax/Bak | Murine leukemia cell line | Bax/Bak deficient line | |
| SF295 | Human glioblastoma | Poorly primed | Doi: 10.1158/1535-7163.MCT-08-0921 |

*Cell line authentication was performed for the MDA-MB-231 and SF295 cell lines by the Dana-Farber Molecular Biology Core Facility using the STR fingerprint method. All cell lines listed above were documented mycoplasma negative.

**Table S4. BH3 profiling of SAH-MS1 peptides**.

| Peptide | O-Bcl-$x_L$ | O-Bcl-2 | O-Bfl-1 | O-Mcl-1 | H929 | MDA-MB-231 | O-Bax/Bak |
|---|---|---|---|---|---|---|---|
| MS1 | $> 10^{-5}$ | $> 10^{-5}$ | $> 10^{-6}$ | $1.1 \times 10^{-7}$ | $7.5 \times 10^{-6}$ | $> 10^{-6}$ | $> 10^{-6}$ |
| SAH-MS1-11 | $> 10^{-5}$ | $> 10^{-5}$ | $> 10^{-6}$ | $5.3 \times 10^{-9}$ | $2.8 \times 10^{-7}$ | $> 10^{-6}$ | $> 10^{-6}$ |
| SAH-MS1-13 | $> 10^{-6}$ | $> 10^{-6}$ | $> 10^{-6}$ | $2.2 \times 10^{-8}$ | $9.8 \times 10^{-8}$ | $> 10^{-6}$ | $> 10^{-6}$ |
| SAH-MS1-16 | $> 10^{-6}$ | $> 10^{-6}$ | $> 10^{-6}$ | $2.9 \times 10^{-8}$ | $1.2 \times 10^{-7}$ | $> 10^{-6}$ | $> 10^{-6}$ |

EC50 values ([peptide], M) for mitochondrial depolarization induced by SAH-MS1 peptides in the indicated B-ALL cell lines. Peptide sequences are listed in Table 2.

**Table S5. Data and refinement statistics for the Mcl-1:SAH-MS1-14 and Mcl-1:SAH-MS1-18 crystal structures.**

| Data | Value | |
|---|---|---|
| | Mcl-1:SAH-MS1-14<br>5W8F | Mcl-1:SAH-MS1-18<br>5W89 |
| Space group | P 41 21 2 | P 41 21 2 |
| Cell dimensions | | |
| a, b, c (Å) | 46.85, 46.85, 167.44 | 44.51, 56.87, 63.98 |
| $\alpha, \beta, \gamma$ (°) | 90, 90, 90 | 90, 90, 90 |
| Resolution (Å) | 19.61-1.85 | 19.41-1.42 |
| $R_{merge}$ | 0.08 | 0.08 |
| $I / \sigma I$ | 1.44 (at 1.85Å) | 1.71 (at 1.42Å) |
| Completeness (%) | 99.9 | 99.2 |
| $R_{work}$ / $R_{free}$ (%) | 24.4/28.5 | 14.2/18.5 |
| Average B-factor (Å$^2$) | 41.8 | 20.6 |
| Anisotropy | 0.257 | 0.036 |

**Table S6. Sequences and masses of SAH-MS1 peptides.**

| Peptide | Sequence | | Experimental mass |
|---|---|---|---|
| MS1 | Ac- | IWMTQGLRRLGDEINAYYARR | 2623.67 |
| SAH-MS1-1 | Ac- | IWXTQGXRRLGDEINAYYARR | 2629.38 |
| SAH-MS1-2 | Ac- | IWBXQGLXRLGDEINAYYARR | 2598.36 |
| SAH-MS1-3 | Ac- | IWBTQXLRRXGDEINAYYARR | 2685.35 |
| SAH-MS1-4 | Ac- | IWBTQGXRRLXDEINAYYARR | 2685.80 |
| SAH-MS1-5 | Ac- | IWBTQGLXRLGXEINAYYARR | 2584.35 |
| SAH-MS1-6 | Ac- | IWBTQGLRXLGDXINAYYARR | 2570.52 |
| SAH-MS1-7 | Ac- | IWBTQGLRRLXDEIXAYYARR | 2684.41 |
| SAH-MS1-8 | Ac- | IWBTQGLRRLGDXINAXYARR | 2563.37 |
| SAH-MS1-9 | Ac- | IWBTQGLRRLGDEIXAYYXRR | 2670.48 |
| SAH-MS1-10 | Ac- | IWBXQGLXRLGDEINAYYAR | 2442.8 |
| SAH-MS1-11 | Ac- | EIWBXQGLXRLGDEINAYYAR | 2571.78 |
| SAH-MS1-12 | Ac- | EIWBXQGLXRLGDEINAYYA | 2415.77 |
| SAH-MS1-13 | Ac- | IWBXQELXRLGDEINAYYARR | 2670.58 |
| SAH-MS1-14 | Ac- | IWBXQSLXRLGDEINAYYARR | 2628.67 |
| SAH-MS1-15 | Ac- | IWBXQSLXRLGDEINAYYAR | 2472.46 |
| SAH-MS1-16 | Ac- | IWBXQELXRLGDEINAYYAR | 2514.26 |
| SAH-MS1-17 | Ac- | IWBXQGLXRLGDEINARYAR | 2435.73 |
| SAH-MS1-18 | Ac- | IWBXQELXRLGDEINARYAR | 2507.94 |
| BIM SAHB (aa 146-166; 2e-3b staple) | Ac- | IWIXQELXRIGDEFNAYYARR | 2704.33 |
| FITC-SAH-MS1-10 | FITC-β-A | IWBXQGLXRLGDEINAYYAR | 2860.44 |
| FITC-SAH-MS1-11 | FITC-β-A | EIWBXQGLXRLGDEINAYYAR | 2989.23 |
| FITC-SAH-MS1-12 | FITC-β-A | EIWBXQELXRLGDEINAYYA | 2833.17 |
| FITC-SAH-MS1-13 | FITC-β-A | IWBXQELXRLGDEINAYYARR | 3088.34 |
| FITC-SAH-MS1-14 | FITC-β-A | IWBXQSLXRLGDEINAYYARR | 3046.44 |
| FITC-SAH-MS1-15 | FITC-β-A | IWBXQSLXRLGDEINAYYAR | 2890.21 |
| FITC-SAH-MS1-16 | FITC-β-A | IWBXQELXRLGDEINAYYAR | 2932.66 |
| FITC-SAH-MS1-17 | FITC-β-A | IWBXQGLXRLGDEINARYAR | 2853.53 |
| FITC-SAH-MS1-18 | FITC-β-A | IWBXQELXRLGDEINARYAR | 2925.24 |

X = (S)-4-pentenylalanine, B = norleucine (substituted for methionine to optimize activity of the ruthenium catalyst).

**Table S7. Sequences and masses of SAH-MB2 peptides.**

| Peptide | Sequence | | Experimental mass |
|---|---|---|---|
| MB2 | Ac- | IWFAQEIDRIGDEVNAYYARR | 2626.16 |
| SAH-MB2-1 | Ac- | IXFAQXIDRIGDEVNAYYARR | 2561.68 |
| SAH-MB2-2 | Ac- | IWXAQEXDRIGDEVNAYYARR | 2616.88 |
| SAH-MB2-3 | Ac- | IWFXQEIXRIGDEVNAYYARR | 2690.26 |
| SAH-MB2-4 | Ac- | IWFAXEIDXIGDEVNAYYARR | 2592.21 |
| SAH-MB2-5 | Ac- | IWFAQXIDRXGDEVNAYYARR | 2634.54 |
| SAH-MB2-6 | Ac- | IWFAQEXDRIXDEVNAYYARR | 2706.85 |
| SAH-MB2-7 | Ac- | IWFAQEIXRIGXEVNAYYARR | 2646.96 |
| SAH-MB2-8 | Ac- | IWFAQEIDXIGDXVNAYYARR | 2591.47 |
| SAH-MB2-9 | Ac- | IWFAQEIDRIXDEVXAYYARR | 2705.46 |
| SAH-MB2-10 | Ac- | IWFAQEIDRIGXEVNXYYARR | 2690.36 |
| SAH-MB2-11 | Ac- | IWFAQEIDRIGDXVNAXYARR | 2584.84 |
| SAH-MB2-12 | Ac- | IWFAQELDRIGDEVXAYYXRR | 2691.71 |
| SAH-MB2-13 | Ac- | I8FAQELDXIGDEVNAYYARR | 2576.77 |
| SAH-MB2-14 | Ac- | IW8AQELDRXGDEVNAYYARR | 2658.54 |
| SAH-MB2-15 | Ac- | IWF8QELDRIXDEVNAYYARR | 2791.11 |
| SAH-MB2-16 | Ac- | IWFA8ELDRIGXEVNAYYARR | 2676.14 |
| SAH-MB2-17 | Ac- | IWFAQ8LDRIGDXVNAYYARR | 2661.32 |
| SAH-MB2-18 | Ac- | IWFAQE8DRIGDEXNAYYARR | 2691.63 |
| SAH-MB2-19 | Ac- | IWFAQEL8RIGDEVXAYYARR | 2690.23 |
| SAH-MB2-20 | Ac- | IWFAQELDR8GDEVNYXYARR | 2691.81 |
| SAH-MB2-21 | Ac- | IWFAQELDRI8DEVNAYXARR | 2698.30 |
| SAH-MB2-22 | Ac- | IWFAQELDRIGD8VNAAYAXR | 2733.11 |
| FITC-SAH-MB2-1 | FITC-β-A | IXFAQXIDRIGDEVNAYYARR | 2980.63 |
| FITC-SAH-MB2-2 | FITC-β-A | IWXAQEXDRIGDEVNAYYARR | 3034.88 |
| FITC-SAH-MB2-3 | FITC-β-A | IWFXQEIXRIGDEVNAYYAR | 3109.67 |
| FITC-SAH-MB2-4 | FITC-β-A | IWFAXEIDXIGDEVNAYYARR | 3011.22 |
| FITC-SAH-MB2-5 | FITC-β-A | IWFAQXIDRXGDEVNAYYARR | 3052.54 |
| FITC-SAH-MB2-6 | FITC-β-A | IWFAQEXDRIXDEVNAYYARR | 3124.85 |
| FITC-SAH-MB2-7 | FITC-β-A | IWFAQEIXRIGXEVNAYYARR | 3064.96 |
| FITC-SAH-MB2-8 | FITC-β-A | IWFAQEIDXIGDXVNAYYARR | 3009.47 |
| FITC-SAH-MB2-9 | FITC-β-A | IWFAQEIDRIXDEVXAYYARR | 3123.46 |
| FITC-SAH-MB2-10 | FITC-β-A | IWFAQEIDRIGXEVNXYYARR | 3108.32 |
| FITC-SAH-MB2-11 | FITC-β-A | IWFAQEIDRIGDXVNAXYARR | 3002.84 |
| FITC-SAH-MB2-12 | FITC-β-A | IWFAQELDRIGDEVXAYYXRR | 3109.71 |

X = (S)-4-pentenylalanine, 8 = (R)-7-octenylalanine, B = norleucine (substituted for methionine to optimize activity of the ruthenium catalyst).

**Supporting Information References**


1. Fire E, Gullá S V, Grant RA, Keating AE (2010) Mcl-1–Bim complexes accommodate surprising point mutations via minor structural changes. *Protein Sci* 19(3):507–519.

2. Certo M, et al. (2006) Mitochondria primed by death signals determine cellular addiction to antiapoptotic BCL-2 family members. *Cancer Cell* 9(5):351–365.

3. Dutta S, et al. (2010) Determinants of BH3 Binding Specificity for Mcl-1 versus Bcl-xL. *J Mol Biol* 398:747–762.

4. Burke JP, et al. (2015) Discovery of Tricyclic Indoles That Potently Inhibit Mcl-1 Using Fragment-Based Methods and Structure-Based Design. *J Med Chem* 58(9):3794–3805.

5. Pelz NF, et al. (2016) Discovery of 2-Indole-acylsulfonamide Myeloid Cell Leukemia 1 (Mcl-1) Inhibitors Using Fragment-Based Methods. *J Med Chem* 59(5):2054–2066.

6. Leverson JD, et al. (2015) Potent and selective small-molecule MCL-1 inhibitors demonstrate on-target cancer cell killing activity as single agents and in combination with ABT-263 (navitoclax). *Cell Death Dis* 6:e1590.

7. Koss B, et al. (2016) Defining specificity and on-target activity of BH3-mimetics using engineered B-ALL cell lines. *Oncotarget* 7(10):11500–11511.

8. Ryan JA, Brunelle JK, Letai A (2010) Heightened mitochondrial priming is the basis for apoptotic hypersensitivity of CD4+ CD8+ thymocytes. *Proc Natl Acad Sci* 107 (29 ):12895–12900.

9. Lorenzi PL, et al. (2009) DNA Fingerprinting of the NCI-60 Cell Line Panel. *Mol Cancer Ther* 8(4):713–724.